Lateral sensitivity in electron probe microanalysis studied by Monte Carlo simulations involving fluorescence enhancements

M. PETACCIA & G. CASTELLANO (iD)
FaMAF, Universidad Nacional de Córdoba, Instituto de Física Enrique Gaviola, CONICET, Córdoba, Argentina

Summary

In electron probe microanalysis, secondary fluorescence can occur leading to an increase of the volume analysed, degrading the lateral resolution of this technique. An adequate knowledge of the interaction volumes from where the different signals of interest are detected is determinant to estimate the minimum size of the zone that can be characterized. In this work, the size of the signal source volume is surveyed for a wide set of samples at different beam energies. To this aim, the PENELOPE software package was chosen to run Monte Carlo simulations for several experimental situations in order to produce the various lateral radiation distributions of interest. A comparison between the interaction volumes of the different signals was performed by taking into account the different fluorescence enhancement possibilities. An unexpected behaviour was found in the particular cases of aluminium and alumina, where the secondary photons signal exhibits a decreasing trend up to certain beam energy ($\sim$17 keV); this implies that lower beam energies may degrade the lateral resolution of the technique in these materials.

Introduction

Electron probe microanalysis (EPMA) is a powerful technique mainly used to perform elemental quantification of the elements present in a sample. When the incident electron beam hits a material, several interactions take place, inner shell ionization being the most important, since atomic relaxation may result in the emission of characteristic x-rays, the intensity of which can be compared with standards of known composition to conveniently obtain the sample composition (Scott *et al.*, 1995).

The beam electron trajectories are shaped by the numerous inelastic and elastic processes occurring in the sample (Reimer, 1998; Goldstein *et al.*, 2003). Some of the incident

Correspondence to: Gustavo Castellano, FaMAF, Universidad Nacional de Córdoba, Medina Allende s/n, Ciudad Universitaria (5000) Córdoba, Argentina. Tel: +54 351 4334051; fax: +54 351 4334054; e-mail: gcas@famaf.unc.edu.ar

electrons are eventually scattered at angles higher than 90°— maybe after multiple interactions—and they abandon the target; these backscattered electrons are used to form images that give chemical contrast information.

As compared to other analytical techniques, an important EPMA advantage is its very good lateral resolution. Due to inelastic scattering, primary electrons suffer a gradual energy loss, for which they bear a finite range of 10 nm–10 μm depending on the beam energy and the material density. The region from where the detected signal originates is called the signal source volume and depends on where the corresponding interactions take place: this volume limits the lateral resolution of this technique.

Characteristic x-rays are mainly produced in the volume where the energy of the primary electrons exceeds the inner shell ionization energy of the atom shell involved. However, secondary fluorescence can occur: in some cases, continuum photons or x-rays produced by atoms of type 'a' can be absorbed by atoms of type 'b', the consequence of such an absorption being a secondary x-ray emission or x-ray fluorescence. This enhancement is normally considered using the primary and secondary intensities, I_{prim} and I_{sec}, by assessing the fluorescence correction factor $F = 1 + I_{sec}/I_{prim}$ (Scott *et al.*, 1995). The signal source volume when secondary fluorescence is considered depends on the absorption of primary as well as secondary radiation and can exceed the range of the electrons.

For an electron beam normal to the surface of a sample, the maximum width of the signal source volume projected towards the surface of the material is a reasonable first approximation for the lateral resolution of the technique: the x-ray production induced by primary electrons is limited by the size of this signal source volume. However, x-rays are more penetrating than electrons and therefore the interaction volume associated with secondary fluorescence (by characteristic photons or by bremsstrahlung) is larger, which obviously degrades the spatial resolution.

Secondary fluorescence cannot always be disregarded, particularly that induced by bremsstrahlung which is always present (Petaccia *et al.*, 2016). In addition, this enhancement

can be especially important in the neighbourhood of an interface, because the signal on one side can be detected although the primary electrons are only transported around the beam spot on the other side. Since secondary photons cannot be distinguished from the total recorded radiation, Monte Carlo simulation becomes an essential tool to study this effect. The simulation of radiation transport based on the Monte Carlo method consists in generating a particle track as a sequence of free steps governed by the corresponding total and differential cross sections. Each of these stochastic steps ends in an interaction which changes the particle dynamical state, i.e. its direction of movement and its energy, eventually producing secondary particles. If the number of generated tracks is large enough, quantitative information on the transport process may be obtained by averaging over a statistically significant number of trajectories. The PENELOPE routine package (Salvat *et al.*, 2011) has proved to adequately describe EPMA experimental situations (Acosta *et al.*, 1998; Llovet *et al.*, 2003; Salvat *et al.*, 2006), and has been chosen for the simulations carried out here.

In this work, the effect of characteristic as well as continuum secondary fluorescence on the signal source volume is studied for typical experimental situations in EPMA using Monte Carlo simulation. These signal source volumes are compared to that of the primary characteristic emission and also to the volume corresponding to the backscattered electron signal. The comparisons clarified some issues, particularly related to the idea of reducing the signal source volume by lowering the beam energy, as usually suggested in the literature (Newbury, 1990; Goldstein *et al.*, 2003; Gauvin, 2007).

Materials and methods

The main program PENCYL offered by the 2011 distribution of the PENELOPE routine package was modified in order to estimate the size of the signal source volume in EPMA, discriminating the different signal contributions: backscattered electrons, primary photons and secondary photons. This was accomplished by the implementation of a classification system for photons that takes into account the process that originated them, and the last interaction position of the emerging x-rays being recorded in a grid in polar coordinates (before

they abandon the specimen). As in all PENELOPE sample programs, once a primary track is completed, the simulation of second-generation particles begins. Every time a characteristic x-ray is produced after ionization by photons, the developed program classifies it according to its origin, through the particle free label ILB(5) (Salvat *et al.*, 2011), and the final code output are radial distributions of the emitted x-rays per unit area.

Unfortunately, both bremsstrahlung production and ionization by photons are rather unlikely processes, and consequently the production of secondary characteristic radiation is a process that occurs with very low probability; for this reason, it is necessary to make the use of variance reduction techniques, which enable the software to accumulate high statistics within reasonable CPU times. Among the alternatives for variance reduction in the PENELOPE package, interaction forcing was the one chosen for this work since it has proved to efficiently provide adequate results for primary and secondary radiation emission (Petaccia *et al.*, 2016). This approach is based on the multiplication of a very low cross-section (for a particular event) by a factor, IFORCE, artificially increasing its probability, hence producing high statistics related to it. All the distributions of interest are then properly normalized in order not to introduce any bias (Bielajew & Rogers, 1988; Salvat *et al.*, 2011).

The values of the different IFORCE parameters for the present simulations were chosen according to the corresponding materials and interactions, as displayed in Table 1. It is worth mentioning that for beam energies capable of producing a statistically reasonable number of ionizations, the IFORCE parameter was set to 50 for inner-shell ionization (by electrons); as the beam energy was lowered, this parameter was correspondingly increased. In addition, in low atomic number samples where characteristic enhancement was present (geological sample material), the IFORCE parameter for x-ray absorption was raised from 100 to 400, since the fluorescence yield is rather low (aluminium in this case).

For each beam energy and irradiated material, the sample lateral size was chosen to ensure the spreading of the ionizations does not exceed its diameter. In addition, other common cutoff simulation parameters were chosen following a criterion established in previous works (Petaccia *et al.*, 2015, 2016); for

Table 1. The multiplying parameters IFORCE chosen for the simulations run for the present work.

	Inner shell ionization	Bremsstrahlung production	X-ray absorption	Beam energies (keV)
Alumina	100	1000	100	8,10,12,13,15,17.5,20
Aluminium	50	1000	100	8,10,11,12,13,14,15,17.5,20
Copper	50	1000	100	15,20
Copper	200	1000	100	10
Fe(1%)-Ni	200	1000	100	10,15,20
Geological sample	50	1000	400	8,10,12,14,15
Titanium	50	1000	100	10,15,20

example, the absorption energy parameters EABS for photons were always chosen to be slightly below the involved ionization energies for each material. In the case of backscattered electrons, the cutoff energy was set to 50 eV, which is the usual convention taken to discriminate them from secondary electrons (Reimer, 1998).

The criterion followed to provide a quantitative estimate for the volume involved in the emission of each signal consisted in determining the radius of the region that contains 99% of all emitted x-rays. To this aim, the cumulative sum for each distribution was assessed, and this radius was calculated along with its corresponding error through a simple local fitting procedure.

All simulations were run in an Intel Quad Core CPU Q8400 2.66 GHz for 6 h to reach statistical uncertainties below 1%. In some situations, in which the secondary emission probability was very small, 96 h simulations were executed in order to fulfil this requirement.

Results and discussion

Figure 1 shows an example of the radial distributions simulated using the program developed for Ti Kα in a pure titanium sample. Evidently, the region occupied by the secondary ionizations is larger than the one associated with primary ionizations, a behaviour observed in all the studied situations. This plot displays the intensity per unit area distribution, as well as the total intensity emitted from each radius r (the program output multiplied by $2\pi r \Delta r$).

In order to obtain the radius of the cylinder containing the 99% of the emitted x-rays, cumulative distributions were assessed as explained above. Figure 2 shows an example for the case of secondary photons in Ti at 20 keV. The radial bin size Δr was specifically chosen for each simulation to accurately provide a reasonable estimate of the lateral resolution: radial

Fig. 2. Cumulative sum for the secondary intensity in a Ti sample at 20 keV. The horizontal line corresponds to 99% of the cumulative emitted intensity.

bin sizes too large result in data being collected in a few radial channels, whereas too small Δr imply insufficient statistics in the distribution.

In Figure 3, a comparison between the different components of the signal detected in electron microprobe analysis can be seen for a pure aluminium sample. The curves for backscattered electrons and primary photons exhibit the expected behaviour (Goldstein *et al.*, 2003; Piños *et al.*, 2017). At low energies, the signal source volume for secondary photons is clearly larger than the one corresponding to the other signals. It must be emphasized that, in this case, secondary radiation is only generated by ionizations produced by bremsstrahlung, mainly emitted in the direction of movement of the propagating primary electrons; due to the low energy of the incident electrons, these are more likely to be scattered, and bremsstrahlung is therefore emitted in all directions, being able to produce ionizations in aluminium far away from the impact region of the electron beam.
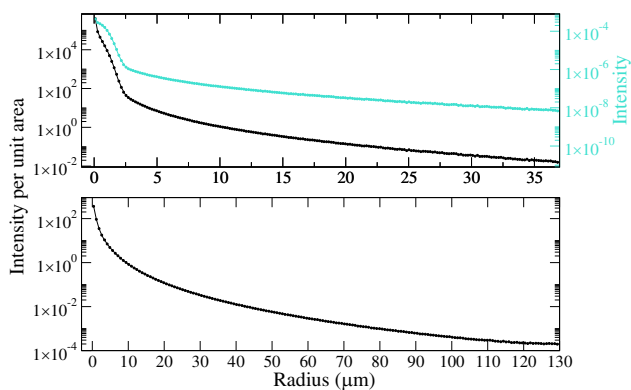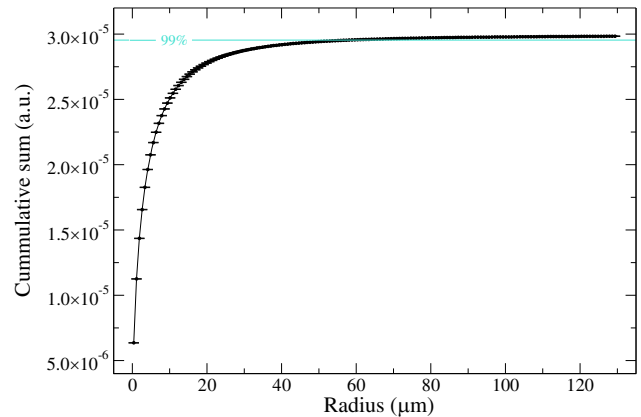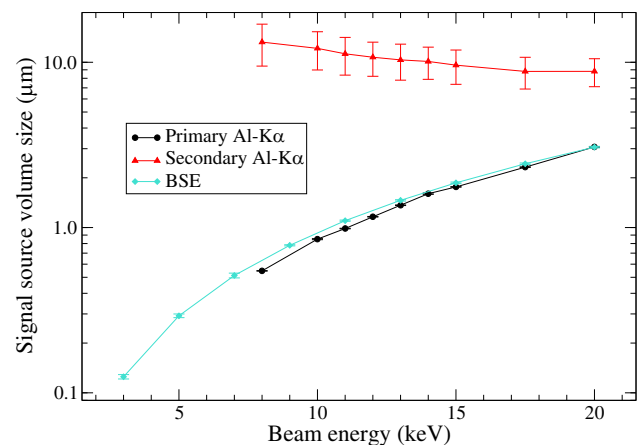

Fig. 1. Radial distribution of primary (top) and secondary (bottom) Kα photons in a Ti sample at 20 keV. In both graphs, the intensity per unit area is displayed; the upper curve (cyan online) corresponds to the total intensity emitted from each ring with radius r and width Δr (right axis scale).

Fig. 3. Size of the signal source volume in pure aluminium for backscattered electrons, primary and secondary photons at several beam energies.

The simulation results show that the secondary photon signal source volume size decreases until a minimum is reached, around 17 keV. This behaviour may be attributed to the different absorption effects experienced by the emitted radiation. These more energetic electrons suffer less elastic interactions along the more superficial layers, penetrating more in the sample and emitting bremsstrahlung mainly to inner material regions; this translates into secondary ionizations close to the direction of incidence. Once the electrons have lost part of their energy, they are more likely to scatter, and bremsstrahlung is emitted more isotropically; however, all of the ionizations generated at this stage are at deeper regions of the sample, and the corresponding secondary photons will suffer larger attenuation when escaping the material.

If the beam energy is incremented above 17 keV, the size of the signal source volume for secondary photons increases until it bears similar values to the interaction volumes of the remaining signals. This is a relevant fact because it points out that for these energies secondary fluorescence does not contribute to the degradation of the lateral resolution of this technique. Although electrons are even more penetrating above 17 keV, it is important to note that they also can reach points laterally more distant from the beam spot; therefore, the signal from the impact point may reduce, whereas the secondary intensity emerging from regions quite apart across the sample surface may increase—or be reduced less strongly. Since the signal source volume surveys all regions from where photons emerge, the increasing behaviour obtained in the secondary intensity is the expected trend for high beam electron energies.

To consider a situation in which absorption effects play an important role, an alumina sample was simulated. In this case, the Al atoms are more diluted than in pure aluminium; in addition, oxygen is present as an absorbing element for the Al-Kα line of interest. The results are similar to the ones described before, although it is worth emphasizing that the absorption effect predominates over the dilution of the Al atoms in the sample: the overall effect is a lateral spreading occurring at deeper regions than in pure aluminium, and the signal source volumes sampled are therefore smaller, as shown in Figure 4.

A different behaviour is observed when samples with higher mean atomic number are considered. Figure 5 shows the size of the signal source volume as a function of the beam energy for the different signals emitted from a pure copper sample. The curves for Cu-Kα primary photons and backscattered electrons show the expected behaviour (Goldstein *et al.*, 2003). Due to the increase in the atomic number, the beam electrons suffer many more elastic collisions for all energies than in low atomic number samples and scatter in all directions. In addition, as bremsstrahlung is mainly emitted in the direction of movement of electrons, an isotropic bremsstrahlung emission occurs starting right from below the surface. Bearing in mind the fact that the mean free path for photons is around 10 times larger than the one corresponding to electrons (of sim-
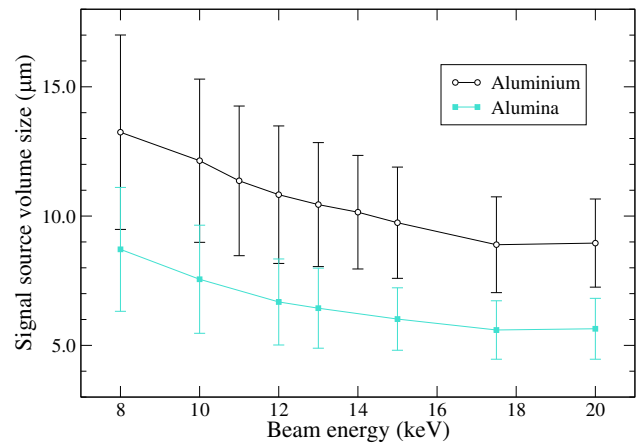

Fig. 4. Comparison of the curves for the size of the signal source volumes for Al-Kα secondary photons between samples of pure aluminium (black circles) and alumina (grey (cyan online) squares) as a function of the electron beam energy.
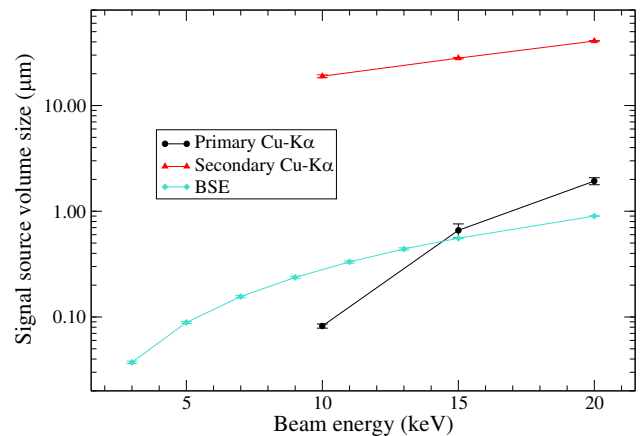

Fig. 5. Size of the signal source volumes for the different components of the signal detected in EPMA for a pure Cu sample at several beam energies.

ilar energy) then, ionizations caused by bremsstrahlung are distributed at characteristic lengths 10 times larger than those associated with electrons; this is clearly evidenced in Figure 5.

In those cases involving an important characteristic enhancement, Fe(1%)-Ni alloy in this study, the curves of size of the signal source volume exhibit a behaviour similar to the ones corresponding to copper, although differences arise in the magnitude of the secondary radiation volume which is several times greater than the values for copper and titanium, as displayed in Figure 6. It is worth mentioning that, for this particular alloy the secondary fluorescence correction due to characteristic FeKα-NiK enhancement may add up to 30% ($F \sim 1.3$) at 15 keV (Petaccia *et al.*, 2015). The signal source volumes for these enhancements are so different due to the fact that characteristic emission after ionization is isotropic, and Ni-Kα photons can be emitted in any direction from shallow depths, unlike bremsstrahlung emission, which is mainly inwards in the first interactions undergone
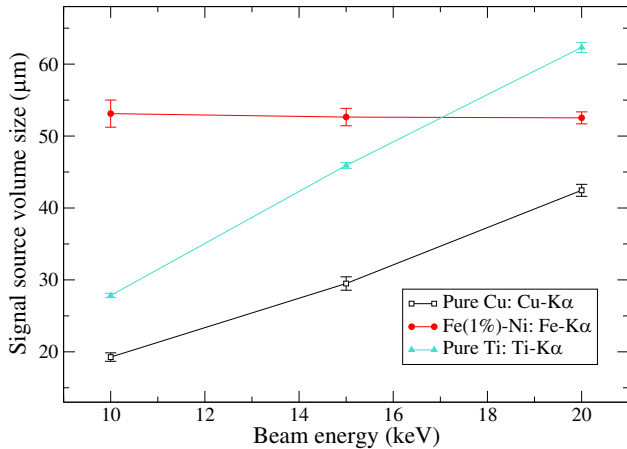
Fig. 6. Comparison of the signal source volume size for secondary radiation in samples of: Cu, Fe(1%)-Ni and Ti as a function of beam energy.
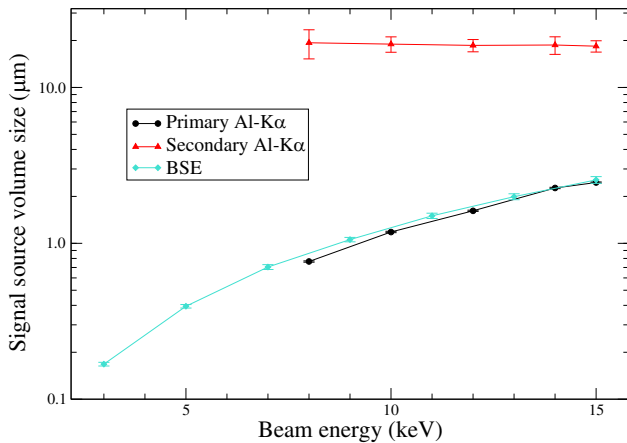

Fig. 7. Size of the signal source volumes for $Al_2O_3(5\%)$-SiO_2 as a function of beam energy.

by the beam electrons, as discussed above. These Ni-Kα x-rays are capable to ionize Fe atoms whose characteristic emission undergoes slight absorption, contributing with an important amount to the Fe-Kα signal source volume from regions well apart from the beam impact point.

A more complex situation can occur in a sample where absorption and enhancement effects are equally important. This is the case of many geological samples, which have been simulated in this work using a sample of chemical composition given by: $Al_2O_3(5\%)$-SiO_2. The signal source volumes for the different signals are shown in Figure 7. In this situation, characteristic Si and bremsstrahlung photons can both ionize Al atoms. The number of continuum photons will be similar to that in the alumina case due to the small difference in the mean atomic number between both samples; as discussed earlier, the alumina sample shows a minimum around 17 keV that has disappeared for the geological sample (Fig. 7). To explain this, characteristic enhancement must be considered: Si

Table 2. Overall signal source volume size for four limiting situations at 15 keV beam energy.

	r_{prim} (μm)	r_{sec} (μm)	F	$r_{overall}$ (μm)
Aluminium	1.76	9.61	1.015	1.88
Copper	0.660	28.1	1.057	2.14
Fe(1%)-Ni	0.479	52.6	1.325	13.36
Geological sample	2.45	18.4	1.039	3.06

primary photons are produced in a volume similar to that for backscattered electrons, being able to propagate in all directions, particularly laterally, which allows them to efficiently ionize Al far away from the impact point; this contribution of secondary photons is more important than the one produced by bremsstrahlung, which is not only lower but also suffers an important attenuation because of the deep regions where it originates, as explained above.

It must be emphasized that in order to obtain a proper estimate of the overall signal source volume size, the corresponding fluorescence correction factor F must be taken into account: if the secondary enhancement is important, the signal source volume for secondary radiation (r_{sec}) will strongly influence the overall lateral resolution; on the contrary for negligible enhancements, only the primary signal source volume size (r_{prim}) will be relevant. A raw estimate for the overall lateral sensitivity may be furnished by properly averaging these contributions:

$$r_{overall} = \frac{r_{prim} + r_{sec}(F - 1)}{F}.$$

Table 2 shows four limiting situations where only bremsstrahlung enhancement is present but negligible (Al), not negligible (Cu), bremsstrahlung as well as characteristic enhancements are important (Fe(1%)-Ni alloy) and finally the geological sample with both enhancements present but too small. Although in some cases the F factor may result small, it must be borne in mind that special care must be taken when analyzing regions neighbouring an interface limiting a material where enhancement can occur.

It is worth mentioning that these r_{prim} values roughly agree with the estimates provided by Pinard & Richter (2014), and also by the approach given by Castaing (1952), as recently suggested by Merlet & Llovet (2012). However, the important situations in which secondary enhancement is present have not been dealt with previously.

Conclusions

The effect of secondary fluorescence on the signal source volume size was studied for typical experimental situations in EPMA using Monte Carlo simulation. To this aim, the main program PENCYL from the PENELOPE 2011 distribution was modified in order to obtain the lateral distribution of emitted

photons. The primary and secondary radiation signal source volumes were compared, exhibiting the expected behaviour; in addition, the primary signal source volume is observed to be slightly smaller than the corresponding to that of backscattered electrons.

In the particular situation of aluminium and alumina, the secondary photons signal exhibits a decreasing trend up to certain beam energy (∼17 keV), from which it starts to grow and blend together with the signal source volumes of the remaining signals. This behaviour, different from the one normally expected, implies that lower beam energies may degrade the lateral resolution of the technique in these materials. For higher atomic numbers, the secondary radiation signal source volume is approximately 10 times larger that the one corresponding to primary radiation, as expected from the corresponding mean free path magnitude analysis. Nevertheless, it must be taken into account that the influence of this secondary signal source volume on the overall lateral sensitivity is always governed by the importance of the F correction factor.

Acknowledgement

References

Acosta, E., Llovet, X., Coleoni, E., Riveros, J.A. & Salvat, F. (1998) Monte Carlo simulation of x-ray emission by kilovolt electron bombardment. *J. Appl. Phys.* **83**(11), 6038–6049.

Bielajew, A. & Rogers, D. (1988) Variance-reduction techniques. *Monte Carlo Transport of Electrons and Photons* (eds. T.M. Jenkins, W.R. Nelson & A. Rindi), pp. 407–419. Springer, Germany.

Castaing, R. (1952) *Application des sondes électroniques à une méthode d'analyse ponctuelle chimique et cristallographique*. PhD Thesis, University of Paris, Publication ONERA no. 55.

Gauvin, R. (2007) A universal equation for the emission range of x rays from bulk specimens. *Microsc. Microanal.* **13**(05), 354–357.

Goldstein, J., Newbury, D., Joy, D., Lyman, C., Echlin, P., Lifshin, E., Sawyer, L. & Michael, J. (2003) *Scanning Electron Microscopy and X-ray Microanalysis*. Kluwer Academic, Plenum Publishers, New York.

Llovet, X., Sorbier, L., Campos, C., Acosta, E. & Salvat, F. (2003) Monte Carlo simulation of x-ray spectra generated by kilo-electron-volt electrons. *J. Appl. Phys.* **93**(7), 3844–3851.

Merlet, C. & Llovet, X. (2012) Uncertainty and capability of quantitative EPMA at low voltage—a review. *IOP Conf. Ser.: Mater. Sci. Eng.* **32**(1), 012016-1–012016-15.

Newbury, D. (1990) Microanalysis to nanoanalysis: measuring composition at high spatial resolution. *Nanotechnology* **1**(2), 103–130.

Petaccia, M., Segui, S. & Castellano, G. (2015) Monte Carlo simulation of characteristic secondary fluorescence in electron probe microanalysis of homogeneous samples using the splitting technique. *Microsc. Microanal.* **21**, 753–758.

Petaccia, M., Segui, S. & Castellano, G. (2016) Bremsstrahlung enhancement in electron probe microanalysis for homogeneous samples using Monte Carlo simulation. *J. Microsc.* **264**(2), 153–158.

Pinard, P. & Richter, S. (2014) Improving the quantification at high spatial resolution using a field emission electron microprobe. *IOP Conf. Ser.: Mater. Sci. Eng.* **55**(1), 012016-1–012016-16.

Piños, J., Mikmeková, V. & Frank, L. (2017) About the information depth of backscattered electron imaging. *J. Microsc.* **266**(3), 335–342.

Reimer, L. (1998) *Scanning Electron Microscopy: Physics of Image Formation and Microanalysis*. Springer, Germany.

Salvat, F., Fernández-Varea, J. & Sempau, J. (2011) PENELOPE 2011: a code system for Monte Carlo simulation of electron and photon transport. *Issy les Moulineau*, OECD Nuclear Energy Agency, France.

Salvat, F., Llovet, X., Fernández-Varea, J. & Sempau, J. (2006) Monte Carlo simulation in electron probe microanalysis. Comparison of different simulation algorithms. *Microchim. Acta* **155**(1–2), 67–74.

Scott, V., Love, G. & Reed, S. (1995) *Quantitative Electron-Probe MicroAnalysis*. Ellis Horwood Ltd., New York.